Check for updates

View Article Online
View Journal

Journal of
Materials Chemistry A

Materials for energy and sustainability

Accepted Manuscript

This article can be cited before page numbers have been issued, to do this please use: H. Yang, Q. Wang, T. D. Pham, Z. Wang, H. Xie, Y. Xu, F. Formalik, D. M. Proserpio, C. L. L. Stern, A. Li, X. C. Krull, A. Cooper, R. Q. Snurr and J. T. Hupp, *J. Mater. Chem. A*, 2026, DOI: 10.1039/D6TA02142E.

This is an Accepted Manuscript, which has been through the Royal Society of Chemistry peer review process and has been accepted for publication.

Accepted Manuscripts are published online shortly after acceptance, before technical editing, formatting and proof reading. Using this free service, authors can make their results available to the community, in citable form, before we publish the edited article. We will replace this Accepted Manuscript with the edited and formatted Advance Article as soon as it is available.

You can find more information about Accepted Manuscripts in the Information for Authors.

Please note that technical editing may introduce minor changes to the text and/or graphics, which may alter content. The journal's standard Terms & Conditions and the Ethical guidelines still apply. In no event shall the Royal Society of Chemistry be held responsible for any errors or omissions in this Accepted Manuscript or any consequences arising from the use of any information it contains.

ROYAL SOCIETY OF CHEMISTRY

rsc.li/materials-a

View Article Online
DOI: 10.1039/D6TA02142E

ARTICLE

Side-Arm Sterics Direct Conformation, Topology, and Function in Zirconium Metal–Organic Frameworks

Received 00th January 20xx,
Accepted 00th January 20xx

DOI: 10.1039/x0xx00000x

Haofan Yang,[1] Qianhui Wang,[1] Thang D. Pham,[2] Zhiwei Wang,[1] Haomiao Xie,[1] Yongjie Xu,[3] Filip Formalik,[2,4] Davide M. Proserpio,[5] Charlotte L. Stern,[1] Alice Li,[1] Xavier C. Krull,[1] Andrew I. Cooper,[3] Randall Q. Snurr,[2] and Joseph T. Hupp[1]

While steric control of linker conformation has proven effective for accessing new Zr-MOF structures, existing strategies have largely relied on modification of the linker core—an approach that intrinsically couples steric effects to framework connectivity, limits available functionalization sites, and often requires complex synthesis, particularly for high-connectivity linkers. Here, we introduce a conceptually distinct and adaptable strategy for topological control based on steric modulation through side-arm functionalization, which enables independent steric tuning without altering linker connectivity while remaining synthetically simple. Six amide or cyano groups positioned on the ligand side arms act as unconventional steric units to induce isolable conformational variability. This design enables the linker to flex and twist, guiding the formation of two isostructural Zr-MOFs, AM-Zr-1 and CN-Zr-1, adopting the rare underlying net 6,8-c *nuh*1 (or 3,8-c *nuh*2) with highly distorted, topologically complex porous architectures. Despite their identical connectivity, AM-Zr-1 generates a geometrically unique amide pocket that enhances CO_2 binding and affords higher CO_2/N_2 and CO_2/CH_4 selectivity, whereas the less bulky cyano substituents confer a more extended conformation to CN-Zr-1, resulting in higher surface area and H_2 uptake. These findings highlight steric side-arm functionalization as a simple yet versatile strategy for tuning Zr-MOF topology and function.

Introduction

Metal–organic frameworks (MOFs) are designable porous crystalline materials constructed from metal-containing "nodes" and multitopic organic "linkers".[1, 2] Zirconium MOFs featuring oxy-anion-terminated linkers are of substantial interest due to: a) their high stability, deriving from strong Zr–O coordination bonds, b) the preference of Zr(IV) for coordination of eight atoms, and c) their propensity to form hexa-zirconium/oxy node cores that can connect to as many twelve chelating or bridging linkers and nonstructural ligands.[3, 4] Since the first synthesis of a Zr-MOF in 2008 (UiO-66),[5] many successful efforts have been made to develop examples exhibiting ample & broad structural diversity, outstanding chemical stability, and intriguing functional properties.[3, 6-10] Nevertheless, discovery of new structures that exploit new topologies is desirable and, indeed, essential for extending, expanding, and enhancing potential applications and for deepening our collective understanding of fundamental correlations between framework structure and properties.[11]

The topological and structural features of MOFs are typically defined and controlled by the geometry and coordination number of the selected metal nodes and organic linkers.[11] However, arbitrariness of metal node formation under various MOF synthetic conditions can induce uncertainty for accessing an expected topology with a desired application. On the other hand, most organic linkers are normally robust in the MOF formation procedure, and more importantly, the geometry and chemical structure of linkers can be well-controlled by various cross-coupling reactions.[12] Therefore, rational design of organic linkers is critical to expanding the diversity of MOF topologies and for modifying the functionality of MOFs with targeted properties and applications.[11, 13]

Steric control over linker conformation holds great potential to enhance the structural and topological diversity of highly connected Zr-MOFs. For example, the introduction of steric hindrance by bulky substituents on the 2- and 2'-positions of a ditopic linker (biphenyl-4,4'-dicarboxylate (BPDC)) forces the two carboxylates and phenyl rings into a perpendicular configuration, leading to the formation of PCN-700 with an 8-connected **bcu** underlying net,[14, 15] rather than UiO-67 with a 12-c **fcu** net.[5] Similarly, for tritopic linkers with the same D_{3h} symmetry, sterically assisted twisting of the three peripheral phenyl rings such that they become perpendicular to the central one in 1,3,5-benzenetribenzoate (BTB) results in the formation

[1] Department of Chemistry, Northwestern University, Evanston, Illinois 60208, United States.
[2] Department of Chemical & Biological Engineering, Northwestern University, Evanston, Illinois 60208, United States.
[3] Materials Innovation Factory & Department of Chemistry, University of Liverpool, 51 Oxford Street, Liverpool L7 3NY, UK.
[4] Department of Micro, Nano, and Biomedical Engineering, Wroclaw University of Science and Technology, 50-370 Wroclaw, Poland.
[5] Dipartimento di Chimica, Università degli studi di MilanoVia Golgi 19, 20133 Milano, Italy.

Open Access Article. Published on 31 March 2026. Downloaded on 4/2/2026 3:01:37 AM.
This article is licensed under a Creative Commons Attribution 3.0 Unported Licence.

Journal of Materials Chemistry A Accepted Manuscript

View Article Online
DOI: 10.1039/D6TA02142E

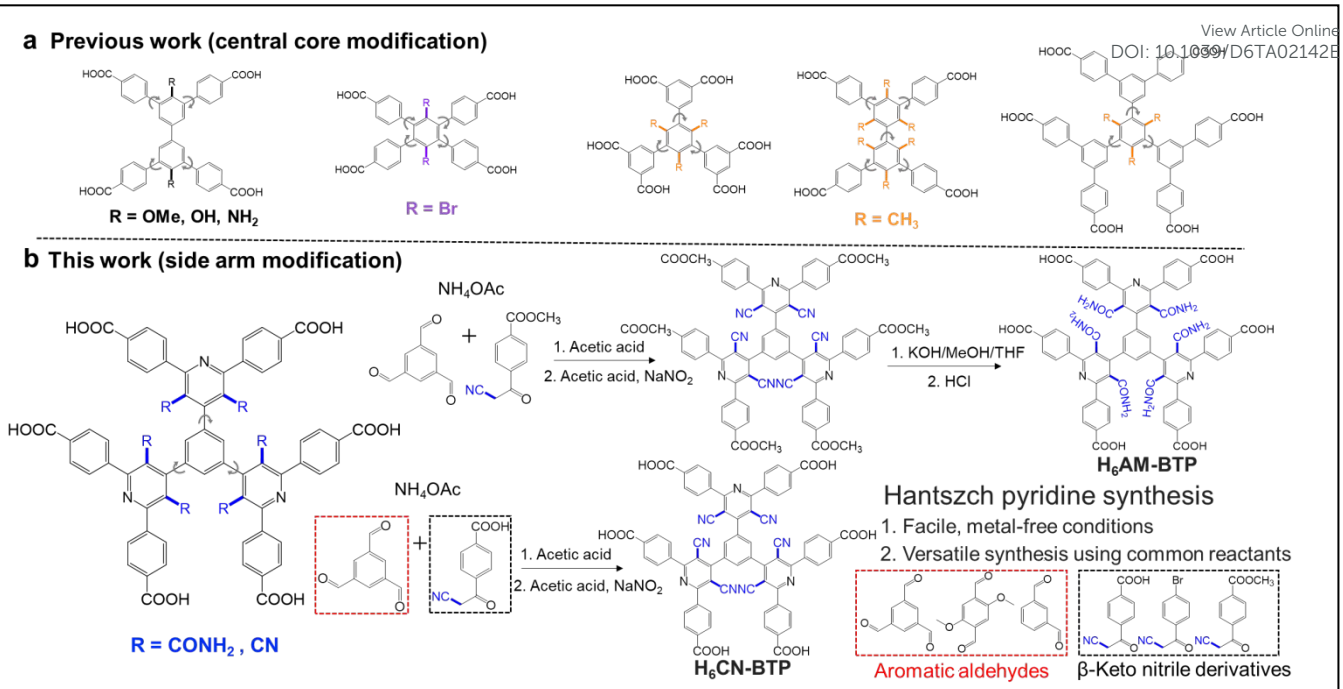

Figure 1. Molecular structural control of conjugate acids of candidate carboxylate linkers by introducing steric hindrance at (a) the aromatic core and (b) the side arms. The reaction scheme illustrates the Hantzsch pyridine synthesis employed to construct the side-arm-functionalized linkers.

of a MOF with 3,8-c **the** net rather than one consisting of 2D 3,6-c **kgd** nets perpendicularly polycatenated.[16, 17] Introduction of steric hindrance to tetratopic linkers has not only contributed to topology diversity but also has enhanced the stability of Zr-MOFs toward moisture due, in part, to ligand rigidification.[18] The strategies used for introducing steric hindrance usually focus on functionalizing the central core of the linker backbone,[18-23] and multi-step syntheses are often required to access these organic linkers with intricate geometry and chemical structure, especially for linkages with higher connectivity, such as hexatopic linkers,[23, 24] Higher connectivity is generally beneficial for topological diversity.[23, 25] Moreover, the linker core typically offers only a limited number of functionalization sites, and modifications at the core can directly affect coordination geometry and connectivity. In contrast, side-arm functionalization introduces additional design handles while preserving core connectivity, providing greater flexibility for steric tuning and opportunities for post-synthetic modification.

Here, we present a new approach to steric control that introduces steric units on linker side arms by a facile and versatile strategy for tuning linker conformation and framework topology in Zr-MOFs. Briefly, we designed two conjugate acids of hexacarboxylated ligands: 4,4',4'',4''',4'''',4'''''-(benzene-1,3,5-triyltris(3,5-dicarbamoylpyridine-4,2,6-triyl))hexabenzoic acid (H_6AM-BTP) and 4,4',4'',4''',4'''',4'''''-(benzene-1,3,5-triyltris(3,5-dicyanopyridine-4,2,6-triyl))hexabenzoic acid (H_6CN-BTP). These ligands incorporate amide or cyano groups on the side arms to introduce steric hindrance and offer conformation flexibility (**Figure 1**). This design leads to the formation of structurally complex 3D Zr-MOFs. The resulting frameworks, AM-Zr-1 (from H_6AM-BTP) and CN-Zr-1 (from H_6CN-BTP), adopt a 6,8-c *nuh*1 (or 3,8-c *nuh*2 underlying net), as calculated by ToposPro 5.5.3.1.[26, 27] Despite sharing the same overall topology, AM-Zr-1 and CN-Zr-1 present different pore chemical environments and display different gas sorption behavior.

Results and discussion

H_6AM-BTP is a newly designed dendritic ligand featuring three chemically identical dicarbamoylpyridine (DCMP) arms and a central benzene core (**Figures 1b** and **2a–d**). Its structural analogue, H_6CN-BTP, incorporates three dicyanopyridine (DCNP) arms, differing only by replacement of the amide groups with cyano substituents (**Figures 1b** and **2e–h**). Despite their structural complexity, H_6AM-BTP and H_6CN-BTP were obtained via the modified Hantzsch pyridine synthesis from readily available aldehyde and β-keto nitriles precursors under metal-free conditions with straightforward purification (**Figure 1b**). The ligands were subsequently characterized by ^{1}H, ^{13}C, and ^{1}H–^{15}N HSQC and HMBC NMR spectroscopy, as well as mass spectrometry (**Figures S1–8** and Supporting Information). Notably, the Hantzsch pyridine synthesis has been shown to be applicable to a wide range of aromatic aldehydes and β-keto nitrile derivatives;[28] This versatility is demonstrated here by employing commonly available aromatic aldehydes and β-keto nitrile derivatives to access the additional side-arm-functionalized molecules, which were characterized by NMR spectroscopy (**Figures 1b** and **S9–14**).

Open Access Article. Published on 31 March 2026. Downloaded on 4/2/2026 3:01:37 AM.
This article is licensed under a Creative Commons Attribution 3.0 Unported Licence.

Journal of Materials Chemistry A Accepted Manuscript

This journal is © The Royal Society of Chemistry 20xx

Please do not adjust margins

View Article Online
DOI: 10.1039/D6TA02142E

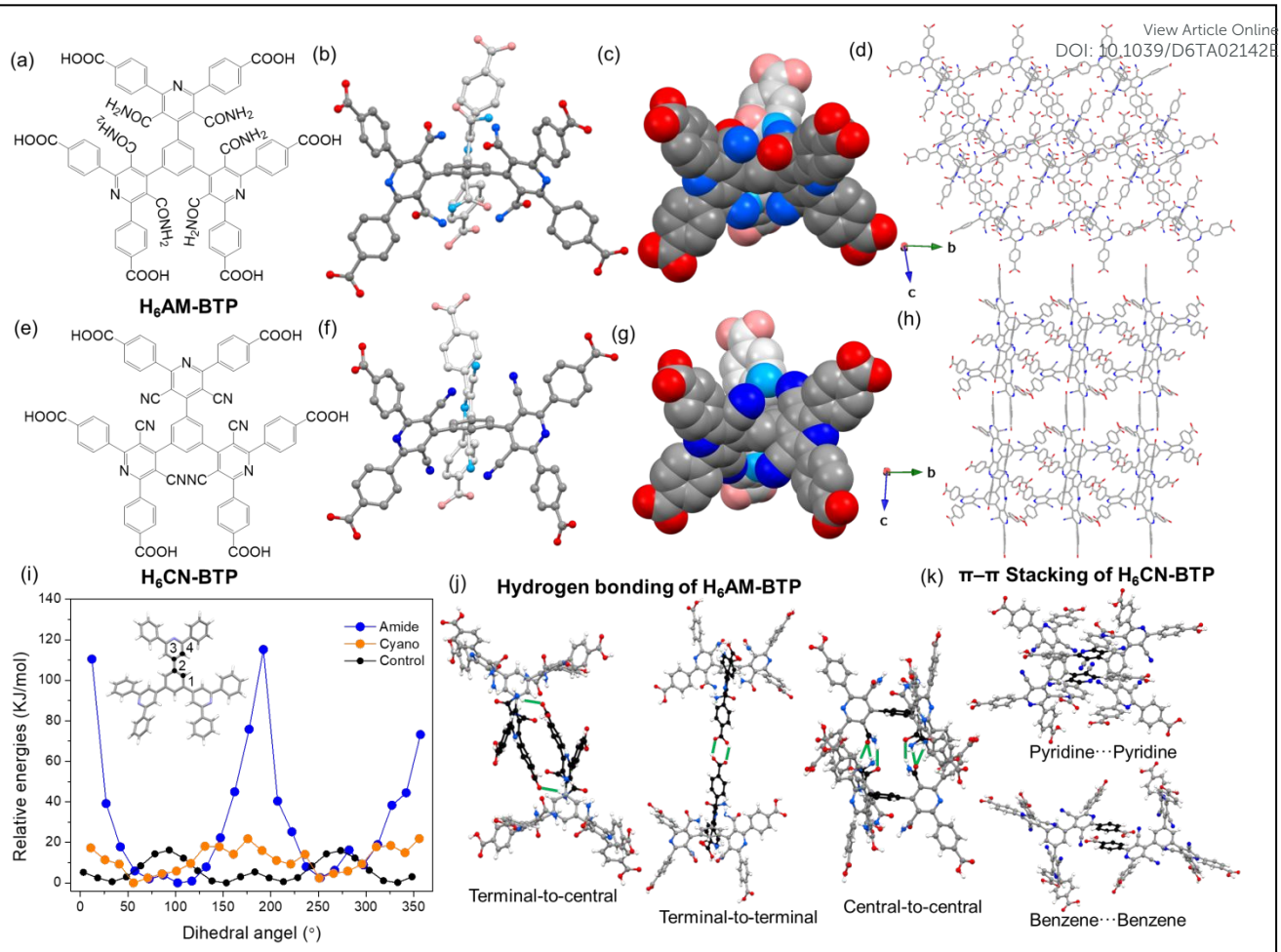

Figure 2. (a) Chemical structure of H_6AM-BTP. (b,c) Ball/stick and space-filling representations of H_6AM-BTP extracted from single-crystal structure of C2. (d) Crystal-packing of C2 viewed from the *a* direction. (e) Chemical structure of H_6CN-BTP. (f,g) Ball/stick and space-filling representations of H_6CN-BTP extracted from single-crystal structure of C3. (h) Crystal-packing of C3 viewed from the *a* direction. (i) Relaxed energy scan of a simplified model of the H_6AM-BTP, H_6CN-BTP, and a control molecule without steric tuning on side arms performed at the M06-L+D3/Def2-TZVP level of theory (details in the Supporting Information, section S3). The dihedral angle is defined by atoms 1-2-3-4 and screened every 15° as illustrated for the control molecule in the inset. (j) Hydrogen bonding of H_6AM-BTP in C2. (k) Benzene···benzene and pyridine···pyridine π stacking of H_6CN-BTP in C3. C, grey and black; N, blue; O, red; H, white. The hydrogen bond is highlighted green, and solvent molecules are omitted for clarity.

To give insight into the steric tuning effect of the amide and cyano groups and the conformational dynamics of the molecules, relaxed energy scans of single (isolated) simplified models of the H_6AM-BTP and H_6CN-BTP molecules were computed using density functional theory (DFT) (In the simplified model, COOH groups were replaced with H atoms for computational efficiency). The highest energies of the simplified model of H_6AM-BTP were observed when the dihedral angle between the arm and the benzene core was approximately 12° and 192°, indicating that a planar conformation is not energetically favorable (**Figure 2i**). The simplified models of H_6CN-BTP displayed a similar profile, with the highest energies near 176° and 356°, consistent with the steric constraints imposed by the cyano groups. Notably, the energy penalty associated with the cyano substituents is smaller than that of the amides (**Figure 2i**), suggesting that the bulkier amides impose stronger steric hindrance, whereas the smaller cyano groups act as weaker steric-tuning elements, affording greater conformational flexibility. In contrast, an unsubstituted analogue lacking amide or cyano groups exhibited relatively low energies at planar conformations (**Figures 2i** and **S15**), highlighting the role of side-arm functionality in enforcing molecular twisting. For comparison, we also examined Me-TDCPB, a previously reported dendritic linker with methyl substituents on the core (**Figure S16**).[29] Although methyl groups provide some steric bias, a simplified model of H_6AM-BTP exhibits higher relative energies near planar geometries than does Me-TDCPB. These results demonstrate that amide and cyano groups on side arms can impose steric modulation, providing a powerful means of conformational control.

Open Access Article. Published on 31 March 2026. Downloaded on 4/2/2026 3:01:37 AM.
This article is licensed under a Creative Commons Attribution 3.0 Unported Licence.

Journal of Materials Chemistry A Accepted Manuscript

Please do not adjust margins

View Article Online
DOI: 10.1039/D6TA02142E

Open Access Article. Published on 31 March 2026. Downloaded on 4/2/2026 3:01:37 AM.
This article is licensed under a Creative Commons Attribution 3.0 Unported Licence.

To gain further insight into molecular conformations, we obtained a single crystal of H_6AM-BTP (C1) from diffusion of ethyl ether into a dimethylacetamide (DMAC) solution. C1 crystallized in the triclinic space group *P*-1 (**Figures S17** and **Table S1**). The steric repulsion arising from the side-arm amide groups, as well as between the amide groups and the central benzene core, forces H_6AM-BTP to adopt a nonplanar structure (**Figure S17**), consistent with the DFT calculation of a single H_6AM-BTP molecule. Although the three DCMP arms are crystallographically distinct, each rotates clockwise relative to the central benzene, adopting dihedral angles of 71–79°. In this structure, the terminal carboxylic acids of all three DCMP arms engage in hydrogen bonding with the central amide groups (**Figures S18–S22**). This "terminal-to-central" assembly decreases pore size and volume for the crystalline molecular (linker) solid, resulting in a maximum pore diameter of 8.05 Å and a solvent-accessible volume of 61% per unit cell. Excluding solvent molecules, these hydrogen bonds give a 6-c **pcu** supramolecular network. A second crystalline form (C2) was obtained from a hexane/acetic acid mixture (**Figures 2a–2d**, **S21**, and **Table S1**). Also crystallizing in *P*-1, C2 retains some conformational features of C1 but displays a distinct arrangement of hydrogen-bonds. The DCMP arms adopt dihedral angles of 60–86°. Two arms participate in the same "terminal-to-central" assembly seen in C1 (**Figures 2j** and **S22**), while the third engages in "terminal-to-terminal" carboxylic acid···carboxylic acid hydrogen bonding, which locally expands the pore. However, the expansion is counterbalanced by dense "central-to-central" amide···amide hydrogen bonding between neighboring molecules, ultimately reducing both the pore volume (40.7%) and the maximum pore diameter (6.38 Å). The overall hydrogen-bonded supramolecular network is built from a highly distorted 6-coordinated geometry, resulting in a rare kind of net called **bcu-x**-6-C2/m.[30]

We next obtained a single crystal of H_6CN-BTP (C3) from diffusion of hexane into an acetic acid solution. C3 crystallized in the triclinic space group *P*-1 (**Figures 2e–2h, S23**, and **Table S1**). Steric repulsion between the cyano substituents and the benzene core similarly enforces a twisted, nonplanar geometry, again consistent with DFT results and analogous to that observed for H_6AM-BTP. The three DCNP arms adopt dihedral angles of 61–85°. These results confirm that both amide and cyano groups on side arms function as steric tuning groups, driving molecular twisting away from planarity. C3 exhibited pore-expanding "terminal-to-terminal" carboxylic acid···carboxylic acid hydrogen bonding (**Figure S24**), but also exhibited pore-contracting dense π–π stacking interactions involving benzene···benzene and pyridine···pyridine pairs (**Figures 2k** and **S25**), yielding a maximum pore diameter of 4.52 Å and a solvent-accessible volume of 31.4% per unit cell. By contrast, no π stacking is observed in C1 or C2, likely because the sterically demanding amides at the molecular center block close aromatic contacts. C1–C3 are all solvates, with carboxylic acid groups engaged in hydrogen bonding to solvent molecules. To expand pore size and volume, we aim to coordinate carboxylates with metal ions, a strategy that simultaneously frees the amide and cyano groups and makes them more accessible.

Solvothermal reaction of $ZrCl_4$ with H_6AM-BTP in the presence of formic acid as a competing reagent ("modulator") in *N*,*N*-diethylformamide (DEF) at 120 °C for 3 days afforded plate-like crystals of AM-Zr-1 (C4) of suitable size for single-crystal X-ray diffraction (SCXRD) analysis (**Figures 3a**, **3b**, and **Table S1**). AM-Zr-1 crystallizes in the orthorhombic space group *P*bam with the formula $[(Zr_6O_4)_3(OH)_{12}(COO)_{12}(AM\text{-}BTP)_4]$. The total solvent-accessible volume in the AM-Zr-1 framework is estimated to be 71% of its unit-cell volume. The combination of cubic 8-connected Zr_6 SBU and 6-connected trigonal-prismatic organic ligand gives rise to a highly distorted framework architecture. Following the guidelines from ToposPro,[26, 27] in a single node cluster description, the structure can be simplified as 6,8-c tetranodal net with point symbol $(4^{11}.6^4)_2(4^{13}.6^2)_2(4^{20}.6^8)_3$ (named *nuh*1) (**Figures S26** and **S27**). When using the all-node cluster description that considers the multibranched nature of the ligand, the framework, now called *nuh*2, is a 10-nodal 3,8-c net with point symbol $(4.8^2)_{12}(4^{12}.8^8.10^8)_3(8^3)_4$ (**Figure 3c**), where each of the two distinct ligands are now mapped on four 3-c nodes. The two nets were deposited by us last year in the TopCryst database.[31] The *nuh* topology has been reported in the peer-reviewed literature only very recently.[32] Its rarity likely arises from the limited availability of highly flexible trigonal-prismatic organic ligands, such as AM-BTP^{6-} and CN-BTP^{6-} in this work and the recently reported BTCH.[32]

Indicative of high flexibility for AM-BTP^{6-}, the unit cell of C4 contains two conformers. In both, the DCMP arms of coordinated AM-BTP^{6-} tilt nearly perpendicularly to the connected benzene core, adopting average dihedral angles of 88.3° and 87.1°, respectively, i.e. larger than those in C1 and C2 (**Figures 3d**, **S28**, and **S29**). This difference is likely a result of geometry constraints of the connection between the Zr_6 cluster and the linkers to match the *nuh*2 net. In addition, the geometry of the sp^2 carbons within the DCMP arms deviates from ideal hybridization, leading to carboxylate O atoms being displaced by up to 0.61 Å out of the pyridine plane and to a large angle distortion index (ADI) for the three N···N···N (pyridine) angles (**Figure 3d**). The larger out-of-plane displacement and ADI in C4 relative to C1 and C2 indicate additional network strain. These unique features result in the formation of highly distorted pores along the *c* direction. The pores define one large distorted hexagonal 1D channel and two small diamond-shaped 1D channels, with pore openings of 15.46, 10.56, and 11.72 Å, respectively (determined by the smallest distance between opposing DCMP pyridine centroids) (**Figure 3e**). To visualize the channels, we implemented an algorithm for pore network compartmentalization using the pyCOSMOS software (**Figures 3f**, **3g**, **S30**, and **S31**).[33] The 1D channels are crossed by twinned trigonal $(Zr_6)_3(AM\text{-}BTP)_2$ and tetragonal $(Zr_6)_2(AM\text{-}BTP)_4$ bipyramid cages (transverse to *c* direction) (**Figures 3h**, **3i**, and **S32**). The separations between four neighboring pyridine centers in one of the $Zr_2(AM\text{-}BTP)_4$ cages are 9.76 and 11.09 Å, respectively. The distance between two centroids of Zr nodes is 17.73 Å (**Figure 3i**).

Journal of Materials Chemistry A Accepted Manuscript

This journal is © The Royal Society of Chemistry 20xx

Please do not adjust margins

View Article Online
DOI: 10.1039/D6TA02142E

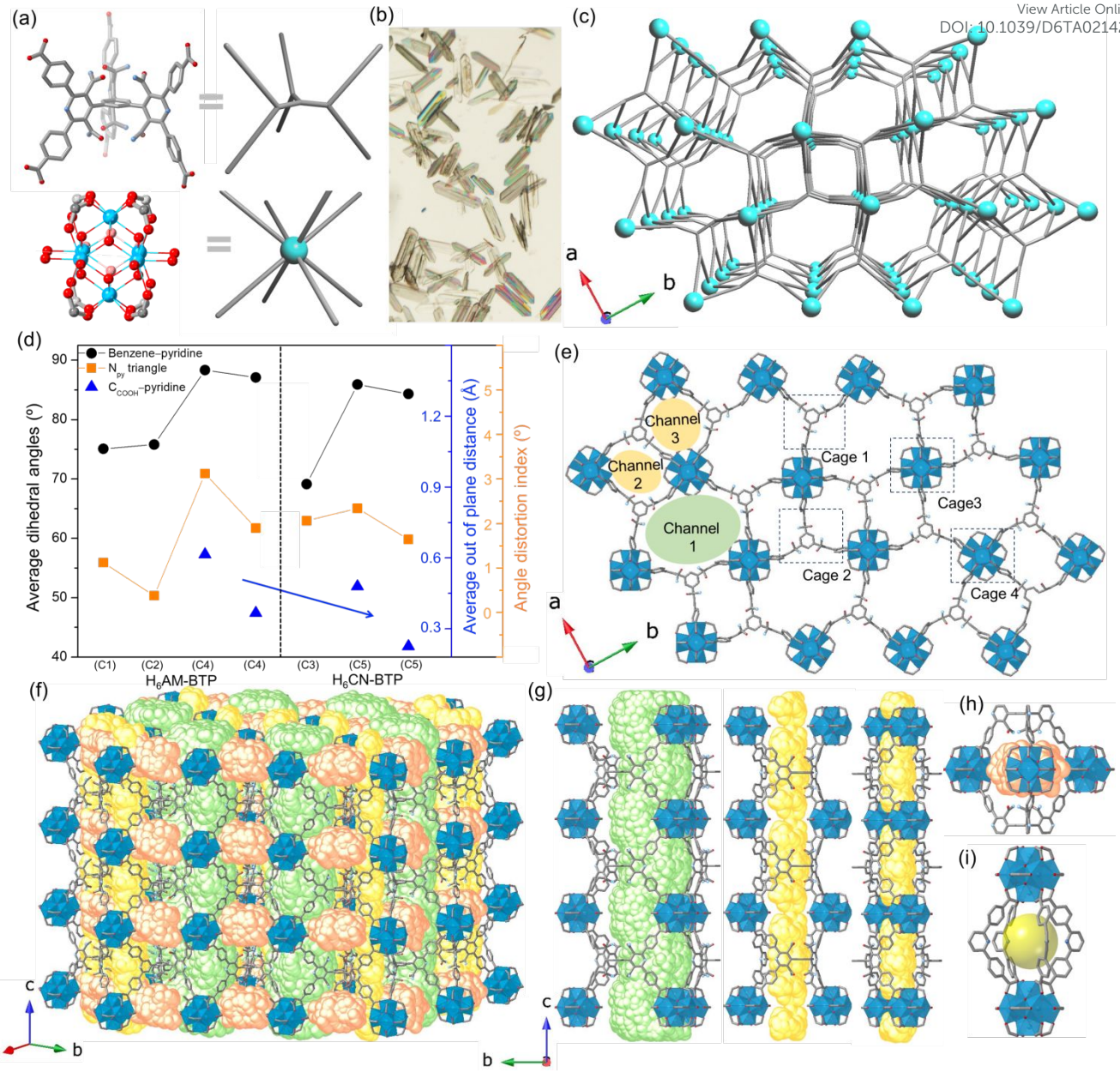

Figure 3. (a) Zr_6 node and organic linker are simplified as blue dot and silver rod. (b) Optical image of single crystals of AM-Zr-1. (c) Underlying net of AM-Zr-1 (*nuh*2) generated by all-node cluster description using ToposPro software. (d) Average dihedral angle between the pyridine and the central benzene plane; angle distortion index (ADI), defined as the root-mean-square deviation of the three N···N···N (pyridine) angles from the ideal 60°; and the average out-of-plane displacement of the carboxylic acid O atoms relative to the pyridine plane, as determined from the crystal structures of C1–C5. (e) Crystal structure of AM-Zr-1 viewed from *c* direction highlighting channel and cage structures. (f) Porosity structure of AM-Zr-1 evaluated by pyCOSMOS software.[33] (g) Distorted-hexagonal (channel 1) and two small diamond-shaped 1D channels (channel 2 and 3) along *c* direction. (h) $(Zr_6)_3$(AM-BTP)$_2$ trigonal bipyramid cage (cage 1) consisting of three Zr_6 nodes and two linkers. (i) $(Zr_6)_2$(AM-BTP)$_4$ tetragonal bipyramid cage (cage 3) consisting of two Zr_6 nodes and four DCMP arms of linkers. Atoms: grey, C; light blue, N; red, O; dark blue, Zr; H is omitted for clarity.

A single crystal of the CN analogue (C5, CN-Zr-1) was obtained from $ZrCl_4$ and H_6CN-BTP in DMF using benzoic acid as the modulator (**Figures S33** and **Table S1**). C5 also crystallizes in *P*bam with formula $[(Zr_6O_4)_3(OH)_{12}(C_6H_5COO)_{12}$(CN-BTP)$_4]$ and is isostructural with C4. Substitution of amide groups by cyano groups leaves the overall composition, connectivity, and topology unchanged. Similar to C4, the unit cell of C5 contains two conformers with average dihedral angles of 85.9° and 84.3°

Open Access Article. Published on 31 March 2026. Downloaded on 4/2/2026 3:01:37 AM.
This article is licensed under a Creative Commons Attribution 3.0 Unported Licence.

Journal of Materials Chemistry A Accepted Manuscript

Please do not adjust margins

View Article Online
DOI: 10.1039/D6TA02142E

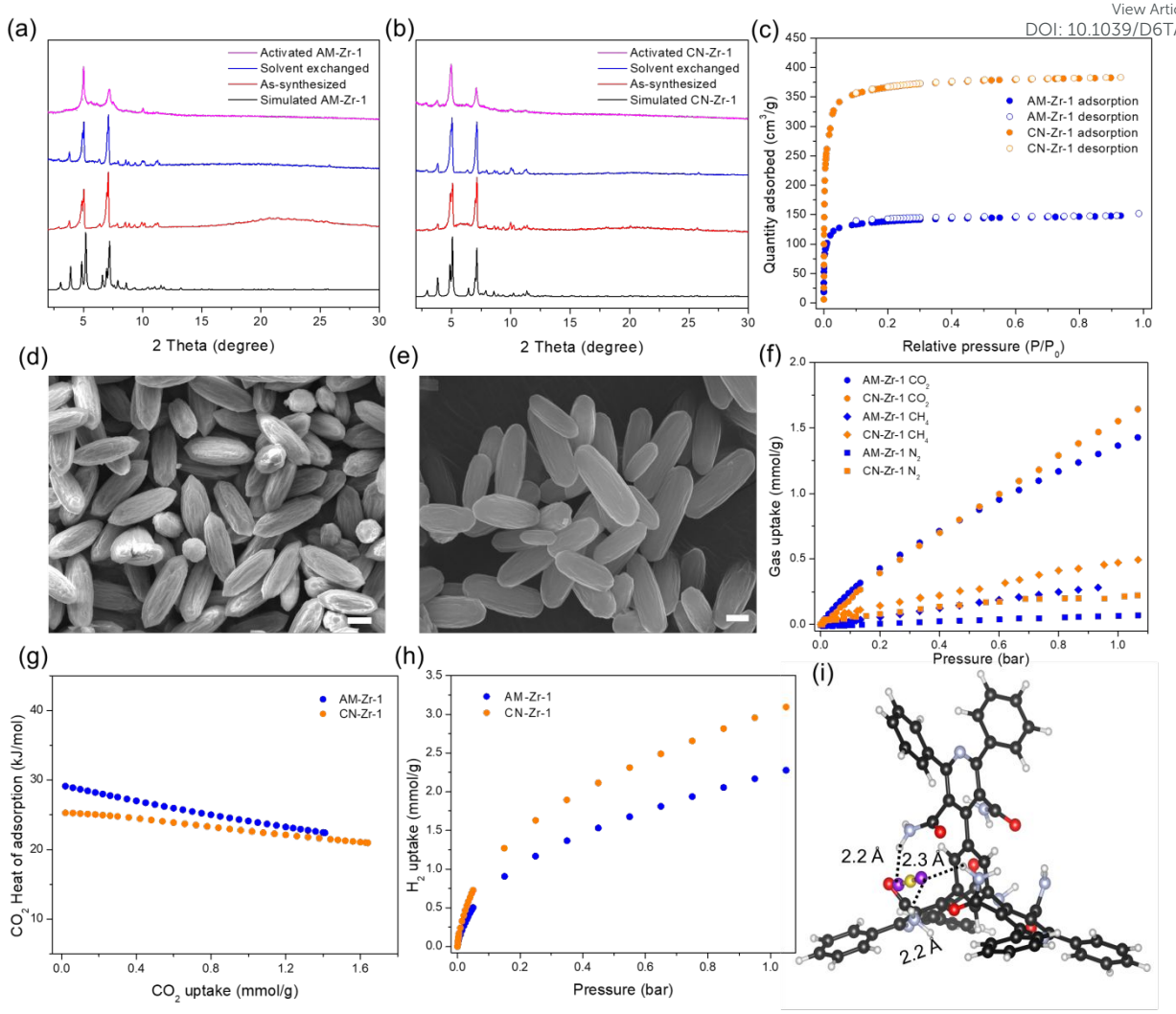

Figure 4. (a) Simulated and experimental PXRD patterns of AM-Zr-1; experimental materials include SC-CO_2 activated, solvent exchanged with acetone, and as-synthesized samples. (b) Simulated and experimental PXRD patterns of CN-Zr-1. (c) N_2 adsorption–desorption isotherms at 77 K. (d,e) SEM image of activated (d) AM-Zr-1 and (e) CN-Zr-1 (scale bar = 1 µm). (f) Experimental adsorption isotherms of CO_2, CH_4, and N_2. (g) CO_2 adsorption enthalpies. (h) H_2 uptake at 77 K. (i) The lowest energy configurations of a CO_2 molecule interacting with the organic linker from DFT at the M06-L+D3/Def2-TZVP level of theory. Color code: H, white; C, black; N, light blue; O, red; C (CO_2), yellow; O (CO_2), purple.

(**Figure 3c**). However, the cell volume (in particular, length in *a* direction) is slightly larger in C5 (**Figure S33)**. Notably, the smaller out-of-plane displacement of the carboxylate O atoms and lower ADI values in C5 relative to C4 indicate less structural distortion within the linker. This reduced distortion correlates with the slightly larger unit cell and reflects a more extended conformation of CN-BTP^{6-} compared to AM-BTP^{6-} (**Figure 3c**), consistent with the reduced steric demand and greater conformational flexibility of the cyano substituents.

The phase purity and structure of AM-Zr-1 and CN-Zr-1 microcrystals synthesized from DMF and formic acid were inferred/confirmed by the agreement of the experimental and calculated powder X-ray diffraction (PXRD) patterns (**Figures 4a** and **4b**). To further validate bulk phase purity, we performed a structureless refinement (Le Bail) of the PXRD data against the single crystal model (**Figures S34** and **S35**), which suggests that the bulk powder is mainly a single-phase product. No obvious structure change of AM-Zr-1 was observed after various liquid solvent exchanges (**Figures 4a** and **S36**), but thermal activation under vacuum led to loss of crystallinity. The flexible feature of AM-BTP^{6-} imposes a challenge in AM-Zr-1 activation, i.e. solvent removal with preservation of porosity, but also engenders restoration of crystallinity when the framework is re-exposed to solvent (**Figure S37**). By using a gentler activation method – supercritical carbon dioxide (SC-CO_2) drying[34-36] – activated AM-Zr-1 preserved crystallinity compared to as-synthesized states and CN-Zr-1 retains better crystallinity (**Figures 4a** and **4b**). The N_2 isotherm of activated samples showed a typical type I profile (**Figure 4c**). CN-Zr-1 displayed a Brunauer–Emmett–Teller (BET) area of 1480 m^2/g, approximately 2.7 times higher than that of

Open Access Article. Published on 31 March 2026. Downloaded on 4/2/2026 3:01:37 AM.
This article is licensed under a Creative Commons Attribution 3.0 Unported Licence.

Journal of Materials Chemistry A Accepted Manuscript

This journal is © The Royal Society of Chemistry 20xx

Please do not adjust margins

View Article Online
DOI: 10.1039/D5TA08142F

Open Access Article. Published on 31 March 2026. Downloaded on 4/2/2026 3:01:37 AM.
This article is licensed under a Creative Commons Attribution 3.0 Unported Licence.

AM-Zr-1 (550 m^2/g). The larger BET of CN-Zr-1 is consistent with higher crystallinity after activation, and possibly because of more extended conformation for CN-BTP^{6-} (**Figure 4b**). The measured surface area of CN-Zr-1 equates to 48.2% of the calculated nitrogen-accessible surface area, whereas that of AM-Zr-1 equates to only 20.7%, suggesting substantial pore collapse in the latter (**Figure S38**). However, the structure can be recovered by heating collapsed AM-Zr-1 in DMF and formic acid (**Figure S39**). Pore size distributions based on a nonlocal density functional theory (NLDFT) model indicated micropores with widths of 11.8 and 14.8 Å for both MOFs, though the total pore volume of CN-Zr-1 (0.51 cm^2/g) is much larger than that of AM-Zr-1 (0.19 cm^2/g) (**Figure S40**). Both AM-Zr-1 and CN-Zr-1 retain their crystallinity after treatment with aqueous solutions of pH 1 HCl and pH 11 NaOH, as well as after boiling in water (**Figure S41**). Thermogravimetric analysis (TGA) showed that both MOFs are stable up to 300 °C (**Figure S42**). Fourier-transform infrared spectra confirmed the presence of amino groups in AM-Zr-1 and cyano groups in CN-Zr-1 (**Figure S43**). Scanning electron microscopy revealed a prolate-shaped microrod morphology for activated AM-Zr-1 and CN-Zr-1 microcrystals with length of 2–4 μm and diameter of around 1 μm (**Figures 4d** and **4e**). Energy-dispersive X-ray spectroscopy (EDS) analysis performed on the selected region showed the presence of N-containing linker and Zr-containing node (**Figures S44** and **S45**). The ^{1}H NMR spectrum of digested AM-Zr-1 showed that no further hydrolysis of amide groups on H_6AM-BTP occurs during MOF synthesis under acidic condition (**Figure S46**). However, ~25% of H_6CN-BTP molecules underwent partial hydrolysis to amide during CN-Zr-1 microcrystals synthesis (formic acid as modulator) (**Figures S47** and **S48**). Hydrolysis of H_6CN-BTP was significantly suppressed when benzoic acid was used as modulator, as evidenced by the digested ^{1}H NMR spectra of CN-Zr-1 single crystals (benzoic acid as modulator) (**Figure S49**). Solvothermally generated formate ions (adventitious capping ligands (nonstructural ligands))[37] were also found: ~4 per node for activated AM-Zr-1 and ~3.7 per node for activated CN-Zr-1 (**Figures S50 and S51**).

MOFs with polar amide groups can enhance CO_2 binding affinity and selectivity.[38-40] The high density of amide functional groups (six per linker) with the unique spatial arrangement (geometrically tight three-amide pocket, AM_3) in AM-Zr-1 motivated us to explore gas sorption selectivity for CO_2 vs. CH_4 and CO_2 vs. N_2. The (single component) CO_2 sorption isotherm of activated AM-Zr-1 showed an uptake of 0.43 mmol g^{-1} at 0.2 bar and 1.36 mmol g^{-1} at 1 bar at 298 K (**Figure 4f**). The CO_2 uptake increased to 2.1 mmol g^{-1} at 1 bar at 278 K (**Figure S52**). By contrast, AM-Zr-1 showed negligible N_2 uptake (0.065 mmol g^{-1} at 1 bar) and low CH_4 uptake (0.28 mmol g^{-1} at 0.93 bar) at 298 K, leading to IAST-predicted selectivities of 220 and 28 for CO_2/N_2 (15/85) and CO_2/CH_4 (50/50) mixtures, respectively, at 298 K and 1 bar (**Figures S53** and **S54**).

CN-Zr-1 showed comparable CO_2 uptake (0.39 mmol g^{-1} at 0.2 bar and 1.55 mmol g^{-1} at 1 bar at 298K), but higher uptakes of N_2 (0.21 mmol g^{-1} at 1 bar) and CH_4 (0.45 mmol g^{-1} at 0.95 bar) relative to AM-Zr-1 (**Figures 4f** and **S52**). Isosteric heats of adsorption for CO_2, calculated using the virial method, were 29 and 22 kJ mol^{-1} for AM-Zr-1 at gas uptakes of 0.02 and 1.41 mmol g^{-1}, respectively, consistently higher than those of CN-Zr-1 across the full loading range (25 kJ mol^{-1} at 0.02 mmol g^{-1}) (**Figures 4g** and **S55**). The decrease of isosteric heat over the entire loading range implies gradual saturation of the strongest binding sites for CO_2. In contrast, the more extended conformation of CN-BTP^{6-} in CN-Zr-1 affords a more robust framework with higher surface area and pore volume. Consequently, CN-Zr-1 displayed greater H_2 uptake (3.09 mmol g^{-1}) than AM-Zr-1 (2.27 mmol g^{-1}) at 1 bar at 77 K (**Figure 4h**).

Cluster DFT calculations were performed to model the interactions between a CO_2 molecule and the MOF (AM-Zr-1) (**Figure S56**). Although a single CO_2 molecule showed a shorter distance to the Zr node than to the amide group (**Figures 4i** and **S57**), in the latter location the CO_2 molecule interacts with the AM_3 pocket through multiple close interactions: O (CO_2)···H (amide) distances of 2.2, 2.3, 2.2 Å; C (CO_2)···O (amide) distances of 2.9, 2.8, 4.7 Å; and C (CO_2)···N (amide) distances of 3.6, 3.5, 4.0 Å) (**Figure 4i**). These close interactions result in higher enthalpies of adsorption for the CO_2 molecule interacting with the amide pocket than the Zr node (–15 versus –13 kJ/mol at 298 K and 1 atm, respectively). Cluster models neglect the dispersion interactions between the CO_2 molecule and the framework atoms that are not represented in the cluster, which may account for the lower heat of adsorption compared to the experiment. However, additional periodic calculations show that the dispersion interaction between the CO_2 molecule and the neglected framework atoms is –24 kJ/mol (**Figure S58**), leading to adsorption enthalpies of –39 kJ/mol for the AM_3 pocket and –37 kJ/mol for the Zr node, both of which align better (but still not exactly) with the experimental heats of adsorption. We speculate that partial pore collapse in experimental samples accounts for the differences with enthalpies from computational modeling of uncollapsed material.

Conclusions

We have demonstrated that steric modulation through side-arm functionalization represents a powerful and versatile design strategy in reticular chemistry. Incorporating amide or cyano substituents into side arms of dendritic hexacarboxylated linkers induces isolable conformational variability that directs the assembly of two isostructural Zr-MOFs, AM-Zr-1 and CN-Zr-1, both adopting the rare *nuh*1 and *nuh*2 topologies. We also found that these steric units modulate not only framework topology but also functional properties. The densely arranged steric units (amide groups) generate a geometrically unique binding pocket that enhances CO_2 affinity and selectivity. On the other hand, the less bulky steric units (cyano groups) yield a more relaxed framework conformation, affording higher surface area and H_2 uptake. These results establish side-arm steric control as a complementary alternative to core substitution for shaping MOF topology and function, providing a versatile route to frameworks with tailored adsorption properties and other applications in the future.

Journal of Materials Chemistry A Accepted Manuscript

Please do not adjust margins

Author contributions

H.Y. designed the study and carried out the experimental work. Q.W. contributed to discussion, characterization, and data analysis. Z.W., H.X., Y.X., and X.C.K. assisted with characterization and analysis. T.D.P. and F.F. performed the simulations. D.M.P. conducted the topology analysis. C.L.S. and A.L. determined the single-crystal structures. A.I.C., R.Q.S., and J.T.H. contributed to scientific discussion and supervised the research. J.T.H. supervised the overall project. All authors discussed the results and commented on the manuscript.

Conflicts of interest

R.Q.S. and J.T.H. have equity interests in NuMat Technologies, a company that commercializes MOFs.

Data availability

The data that support the findings of this study are presented in the paper and the ESI. Deposition numbers 2454893–2454895, 2486952, and 2504783 contain the supplementary crystallographic data for this paper. These data can be obtained free of charge via the joint Cambridge Crystallographic Data Centre (CCDC).

Acknowledgements

R.Q.S. and J.T.H. acknowledge financial support from the U.S. Department of Energy Office of Science, Basic Energy Sciences, Program for Separation Science (DE-FG02-08ER15967) and from Northwestern University. This research used resources of the National Energy Research Scientific Computing Center, a DOE Office of Science User Facility supported by the Office of Science of the U.S. Department of Energy under Contract No. DE-AC02-05CH11231 using NERSC award BES-ERCAP0026793. This research was supported in part through the computational resources and staff contributions provided for the Quest high performance computing facility at Northwestern University which is jointly supported by the Office of the Provost, the Office for Research, and Northwestern University Information Technology. This work made use of the IMSERC Crystallography, MS and NMR facilities at Northwestern University, which has received support from the Soft and Hybrid Nanotechnology Experimental (SHyNE) Resource (RRID:SCR_017874), and Northwestern University. X.C.K. acknowledges partial support from the U.S. Department of Energy through the Office of Science Graduate Student Research (SCGSR) program. D.M.P. thanks Prof. Vladislav A. Blatov at the Samara Center for Theoretical Materials Science for providing the free ToposPro software (https://tospro.com).

References

1 L. E. Kreno, K. Leong, O. K. Farha, M. Allendorf, R. P. Van Duyne and J. T. Hupp, *Chemical Reviews*, 2012, **112**, 1105-1125.

2 H. Furukawa, K. E. Cordova, M. O'Keeffe and O. M. Yaghi, *Science*, 2013, **341**, 1230444.

3 Y. Bai, Y. Dou, L.-H. Xie, W. Rutledge, J.-R. Li and H.-C. Zhou, *Chemical Society Reviews*, 2016, **45**, 2327-2367.

4 S. Yuan, L. Feng, K. Wang, J. Pang, M. Bosch, C. Lollar, Y. Sun, J. Qin, X. Yang, P. Zhang, Q. Wang, L. Zou, Y. Zhang, L. Zhang, Y. Fang, J. Li and H.-C. Zhou, *Advanced Materials*, 2018, **30**, 1704303.

5 J. H. Cavka, S. Jakobsen, U. Olsbye, N. Guillou, C. Lamberti, S. Bordiga and K. P. Lillerud, *Journal of the American Chemical Society*, 2008, **130**, 13850-13851.

6 T. C. Wang, W. Bury, D. A. Gómez-Gualdrón, N. A. Vermeulen, J. E. Mondloch, P. Deria, K. Zhang, P. Z. Moghadam, A. A. Sarjeant, R. Q. Snurr, J. F. Stoddart, J. T. Hupp and O. K. Farha, *Journal of the American Chemical Society*, 2015, **137**, 3585-3591.

7 B. Wang, P. Wang, L.-H. Xie, R.-B. Lin, J. Lv, J.-R. Li and B. Chen, *Nature Communications*, 2019, **10**, 3861.

8 C. Koschnick, M. W. Terban, R. Frison, M. Etter, F. A. Böhm, D. M. Proserpio, S. Krause, R. E. Dinnebier, S. Canossa and B. V. Lotsch, *Journal of the American Chemical Society*, 2023, **145**, 10051-10060.

9 W. Gong, X. Chen, K. M. Fahy, J. Dong, Y. Liu, O. K. Farha and Y. Cui, *Journal of the American Chemical Society*, 2023, **145**, 13869-13878.

10 W. Gong, X. Chen, W. Zhang, K. O. Kirlikovali, B. Nan, Z. Chen, R. Si, Y. Liu, O. K. Farha and Y. Cui, *Journal of the American Chemical Society*, 2022, **144**, 3117-3126.

11 M. Li, D. Li, M. O'Keeffe and O. M. Yaghi, *Chemical Reviews*, 2014, **114**, 1343-1370.

12 D. Zhao, D. J. Timmons, D. Yuan and H.-C. Zhou, *Accounts of Chemical Research*, 2011, **44**, 123-133.

13 L. Feng, Y. Wang, K. Zhang, K. Y. Wang, W. Fan, X. Wang, J. A. Powell, B. Guo, F. Dai, L. Zhang, R. Wang, D. Sun and H.-C. Zhou, *Angewandte Chemie International Edition*, 2019, **58**, 16682-16690.

14 S. Yuan, Y.-P. Chen, J.-S. Qin, W. Lu, L. Zou, Q. Zhang, X. Wang, X. Sun and H.-C. Zhou, *Journal of the American Chemical Society*, 2016, **138**, 8912-8919.

15 S. Yuan, W. Lu, Y.-P. Chen, Q. Zhang, T.-F. Liu, D. Feng, X. Wang, J. Qin and H.-C. Zhou, *Journal of the American Chemical Society*, 2015, **137**, 3177-3180.

16 B. Wang, X.-L. Lv, D. Feng, L.-H. Xie, J. Zhang, M. Li, Y. Xie, J.-R. Li and H.-C. Zhou, *Journal of the American Chemical Society*, 2016, **138**, 6204-6216.

17 R. Wang, Z. Wang, Y. Xu, F. Dai, L. Zhang and D. Sun, *Inorganic Chemistry*, 2014, **53**, 7086-7088.

18 X.-L. Lv, S. Yuan, L.-H. Xie, H. F. Darke, Y. Chen, T. He, C. Dong, B. Wang, Y.-Z. Zhang, J.-R. Li and H.-C. Zhou, *Journal of the American Chemical Society*, 2019, **141**, 10283-10293.

19 X. Song, Y. Wang, C. Wang, D. Wang, G. Zhuang, K. O. Kirlikovali, P. Li and O. K. Farha, *Journal of the American Chemical Society*, 2022, **144**, 10663-10687.

20 J. Pang, S. Yuan, J. Qin, C. Liu, C. Lollar, M. Wu, D. Yuan, H.-C. Zhou and M. Hong, *Journal of the American Chemical Society*, 2017, **139**, 16939-16945.

21 T. Y. Tai, F. Sha, X. Wang, X. Wang, K. Ma, K. O. Kirlikovali, S. Su, T. Islamoglu, S. Kato and O. K. Farha, *Angewandte Chemie International Edition*, 2022, **61**, e202209110.

22 X. Zhao, X. Wang, S. Wang, J. Dou, P. Cui, Z. Chen, D. Sun, X. Wang and D. Sun, *Crystal Growth & Design*, 2012, **12**, 2736-2739.

23 Z. Chen, Ł. J. Weseliński, K. Adil, Y. Belmabkhout, A. Shkurenko, H. Jiang, P. M. Bhatt, V. Guillerm, E. Dauzon, D.-X. Xue, M. O'Keeffe and M. Eddaoudi, *Journal of the American Chemical Society*, 2017, **139**, 3265-3274.

24 O. K. Farha, A. Özgür Yazaydın, I. Eryazici, C. D. Malliakas, B. G. Hauser, M. G. Kanatzidis, S. T. Nguyen, R. Q. Snurr and J. T. Hupp, *Nature Chemistry*, 2010, **2**, 944-948.

View Article Online
DOI: 10.1039/D6TA02142E

Open Access Article. Published on 31 March 2026. Downloaded on 4/2/2026 3:01:37 AM.
This article is licensed under a Creative Commons Attribution 3.0 Unported Licence.

Journal of Materials Chemistry A Accepted Manuscript

This journal is © The Royal Society of Chemistry 20xx

Please do not adjust margins

View Article Online
DOI: 10.1039/D6TA02142E

25 V. Guillerm, Ł. J. Weseliński, Y. Belmabkhout, A. J. Cairns, V. D'elia, Ł. Wojtas, K. Adil and M. Eddaoudi, *Nature Chemistry*, 2014, **6**, 673-680.
26 C. Bonneau, M. O'Keeffe, D. M. Proserpio, V. A. Blatov, S. R. Batten, S. A. Bourne, M. S. Lah, J.-G. Eon, S. T. Hyde, S. B. Wiggin and L. Öhrström, *Crystal Growth & Design*, 2018, **18**, 3411-3418.
27 V. A. Blatov, A. P. Shevchenko and D. M. Proserpio, *Crystal Growth & Design*, 2014, **14**, 3576-3586.
28 X. Li, Y. Che, L. Chen, T. Liu, K. Wang, L. Liu, H. Yang, E. O. Pyzer-Knapp and A. I. Cooper, *Nature Chemistry*, 2024, **16**, 1286-1294.
29 J. Jia, F. Sun, H. Ma, L. Wang, K. Cai, Z. Bian, L. Gao and G. Zhu, *Journal of Materials Chemistry A*, 2013, **1**, 10112-10115.
30 V. A. Blatov, *Foundations of Crystallography*, 2007, **63**, 329-343.
31 A. P. Shevchenko, A. A. Shabalin, I. Y. Karpukhin and V. A. Blatov, *Science and Technology of Advanced Materials: Methods*, 2022, **2**, 250-265.
32 X.-J. Kong, H. Xie, J. Liu, T. He, X. Wang, K. Wang, X. Tang, B. Hou, K. O. Kirlikovali, R. Q. Snurr and O. K. Farha, *Journal of the American Chemical Society*, 2026.
33 S. Parashar and A. V. Neimark, *Journal of Chemical Information and Modeling*, 2024, **64**, 3260-3268.
34 A. P. Nelson, O. K. Farha, K. L. Mulfort and J. T. Hupp, *Journal of the American Chemical Society*, 2009, **131**, 458-460.
35 O. K. Farha and J. T. Hupp, *Accounts of Chemical Research*, 2010, **43**, 1166-1175.
36 Y.-S. Bae, K. L. Mulfort, H. Frost, P. Ryan, S. Punnathanam, L. J. Broadbelt, J. T. Hupp and R. Q. Snurr, *Langmuir*, 2008, **24**, 8592-8598.
37 Z. Lu, J. Liu, X. Zhang, Y. Liao, R. Wang, K. Zhang, J. Lyu, O. K. Farha and J. T. Hupp, *Journal of the American Chemical Society*, 2020, **142**, 21110-21121.
38 B. Zheng, J. Bai, J. Duan, L. Wojtas and M. J. Zaworotko, *Journal of the American Chemical Society*, 2011, **133**, 748-751.
39 C. Chen, M. Zhang, W. Zhang and J. Bai, *Inorganic Chemistry*, 2019, **58**, 2729-2735.
40 X. Song, M. Zhang, C. Chen, J. Duan, W. Zhang, Y. Pan and J. Bai, *Journal of the American Chemical Society*, 2019, **141**, 14539-14543.

Open Access Article. Published on 31 March 2026. Downloaded on 4/2/2026 3:01:37 AM.
This article is licensed under a Creative Commons Attribution 3.0 Unported Licence.

Journal of Materials Chemistry A Accepted Manuscript

Please do not adjust margins

View Article Online
DOI: 10.1039/D6TA02142E

Data availability

The data that support the findings of this study are presented in the paper and the ESI. Deposition numbers 2454893–2454895, 2486952, and 2504783 contain the supplementary crystallographic data for this paper. These data can be obtained free of charge via the joint Cambridge Crystallographic Data Centre (CCDC).

Open Access Article. Published on 31 March 2026. Downloaded on 4/2/2026 3:01:37 AM.
This article is licensed under a Creative Commons Attribution 3.0 Unported Licence.

Journal of Materials Chemistry A Accepted Manuscript